IEEE Access
Multidisciplinary | Rapid Review | Open Access Journal

Received 6 August 2024, accepted 18 August 2024, date of publication 21 August 2024, date of current version 30 August 2024.

Digital Object Identifier 10.1109/ACCESS.2024.3446967

RESEARCH ARTICLE

Optimization Strategy of Wind Power Curtailment Under LVRT Operation

SANGWON KIM, (Member, IEEE)
Department of Electrical, Electronic, and Computer Engineering, University of Ulsan, Ulsan 44610, South Korea
e-mail: angwon22@ulsan.ac.kr

This work was supported by the National Research Foundation of Korea (NRF) through Korean Government (MSIT) under Grant RS-2022-00165574.

ABSTRACT A novel wind power curtailment optimization method considering low-voltage ride through (LVRT) operation is developed. The reserve capacity of wind generation for reactive power output is necessary to ensure the proper operation of a wind power plant (WPP) when a voltage drop occurs. In this context, the active power production of the wind power plant is curtailed to obtain the reactive power output capacity. On the contrary, this curtailed wind operation leads to an increased power system fuel cost. Considering these aspects, the proposed methodology can determine the optimal wind curtailment level by the optimal power flow (OPF) formulation. The wind-side bus voltage during the low-voltage condition is incorporated as an additional inequality constraint. Furthermore, the wind-side grid frequency decreases due to the reduced power production of the wind power plant after a fault occurrence. A primary frequency controller can be implemented in the WPP model to alleviate this frequency drop. The proposed method is evaluated based on the Western System Coordinating Council (WSCC) three-generator nine-bus and IEEE 39-bus power system models. The relationships among the wind power curtailment ratio, wind-side bus voltage constraints, and wind power plant capacity are analyzed.

INDEX TERMS Low-voltage ride through, optimal power flow, primary frequency control, voltage constraint, wind power curtailment.

NOMEMCLATURE

ABBREVIATIONS

AVR	Automatic voltage regulator.
DFIG	Doubly-fed induction generator.
GOV	Turbine speed governor.
HVDC	High-voltage direct current.
LVRT	Low-voltage ride through.
MPPT	Maximum power point tracking.
OPF	Optimal power flow.
PCC	Point of common coupling.
PMSG	Permanent magnet synchronous generator.
VSC	Voltage-source converter.
WPP	Wind power plant.

PARAMETERS

A_G, B_G, C_G	Fuel cost coefficients of generators.
$E(i)$	Set of buses connected to bus i.
P, Q	Active and reactive power injection at a bus.
f_{WF}	Frequency measurement of wind-side PCC bus.
C_{WT}	Power coefficient of wind model.
H_{WT}	Inertia constant of wind model.
P_{WT}	Active power production of wind model.
P_{MPPT}	Power output by wind MPPT control.
P_f	Power adjustment for frequency support.
$P_{m,WT}$	Mechanical power input of wind model.
P_{max}	Rated active power production of wind model.
$P_{WT,min}$	Minimum active power output of wind model.
P_G	Active power output of generator.

The associate editor coordinating the review of this manuscript and approving it for publication was Yifan Zhou.

P_L	Active power consumption by a load.
Q_G	Reactive power output of generator.
Q_L	Reactive power consumption by a load.
S_G	Apparent power output of generator.
Q_{WT}	Reactive power output of wind model.
R_{WT}	Ratio of curtailed wind power output.
V_{WT}	PCC bus voltage of wind model.
V_{AC}	AC bus voltage magnitude.
ω_r	Rotational speed of wind model.
k_f	Droop constant of frequency support.
g	Equality constraints.
h	Inequality constraints.
u	Vector of control variables.
x	Vector of state variables.
P_{line}	Transmission line active power flow.
R_{Tap}	Tap transformer ratio.
K	Set of contingencies.

INDICES

0	Initial value of a parameter.
G	Indices of synchronous generators.
i, j	buses in a power system model.
k	Contingency k.
max	Maximum value of a parameter.
min	Minimum value of a parameter.

I. INTRODUCTION

A. RESEARCH BACKGROUND

The growth of wind generation is rapidly increasing owing to its technological, environmental, and economic advantages. In this context, various issues related to large-scale wind power plant (WPP) integration into power systems have recently been assessed. Low-voltage ride through (LVRT), when a disturbance occurs near the WPP, is the most important topic to be overcome.

Doubly-fed induction generator (DFIG) and permanent magnet synchronous generator (PMSG)-based wind turbines are widely adopted for large-scale WPPs. One of the major advantages of the PMSG-type compared to the DFIG-type is the larger operation range based on full-scale converters [1], [2]. The flexibility of full-scale converter control by the PMSG helps easily satisfies the LVRT scheme [3].

Temporary wind power output reduction occurs during low-voltage operation after a grid-side disturbance. This can lead to a frequency drop near the wind generation. Moreover, this frequency deviation becomes critical if a large-scale WPP is disconnected from the grid-side during a grid-side fault. In order to avoid this phenomenon, many LVRT grid codes require WPPs to be connected to the grid-side during low-voltage operations.

The wind-side voltage should be maintained stably to satisfy the LVRT requirements. In this regard, the reactive power output of the WPPs can be controlled to support the wind-side bus voltage. The reactive power control of the WPPs, depending on the magnitude of the wind-side bus voltage described in FIGURE 1, is widely adopted for dynamic voltage support [4]. If the wind-side bus voltage drops below 0.9 *p.u.*, the wind model starts to produce reactive power to support the voltage. If the voltage magnitude is less than 0.5 *p.u.*, the reactive power production of the wind model reaches the maximum value and no active power is produced.

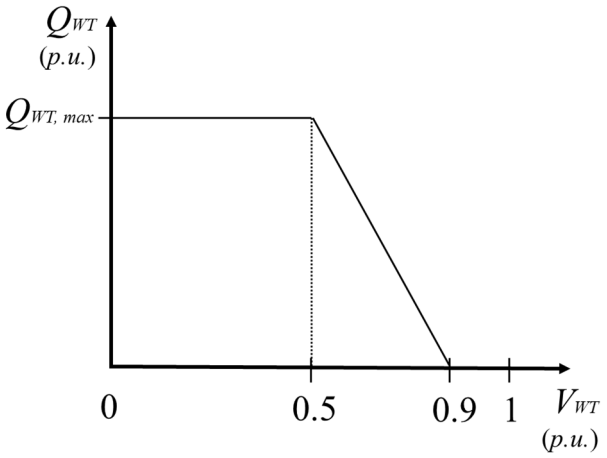

FIGURE 1. Wind-side voltage dependent reactive power control [4].

Nevertheless, this dynamic voltage support is inefficient if the wind-side voltage drop is severe. The controllability of the WPPs is constrained by the current limiters of the converters during the voltage drop. In order to cope with this problem, the contribution of reactive power control by the WPPs during the steady-state can be devised.

However, the active power output of the WPPs should be curtailed to secure their steady-state reactive power output capacity. The necessity of wind power curtailment occurs in case of transmission congestion [5]. Meanwhile, the wind model can support grid-side frequency if the reserve capacity is secured by this wind output suppression.

Nonetheless, this active power curtailment is not beneficial from the perspective of grid-side fuel cost since the fuel cost of the WPPs is low or zero in general, Hence, a method which calculates the optimal curtailment level of the wind generation considering both the stable wind-side bus voltage and the minimum fuel cost is required.

B. LITERATURE REVIEW

Wind power curtailment can be requested by power system operators for various purposes. One of the most popular objectives of the curtailment is power system frequency regulation. The overspeed operation of the pitch-angle and wind rotor control can be applied to secure the reserve margin [6], [7], [8], [9], [10], [11]. Integrated control of the wind power curtailment and automatic generation control for the frequency control is proposed in [12].

Regarding other issues, the improvement in the power system transient stability by wind power suppression is studied in [13]. The reserve capacity obtained by the wind curtailment can provide inertial support in a power system model [14]. Deloaded wind operations for load sharing are suggested

in [15] and [16]. However, none of these studies have investigated the necessity of the wind power curtailment considering LVRT characteristics.

The wind power output suppression of a PMSG-type wind model with LVRT-coordinated control is discussed in [17]. Nevertheless, this wind power curtailment results in an increased operation cost of a power system model. Hence, the proper level of the curtailment should be carefully determined considering the operation cost.

In this context, a formulation to obtain the optimal amount of the wind power curtailment should be developed. For instance, the optimal output results of the deloaded wind generation and thermal units can be calculated by unit commitment [18]. Demand response sources and energy storage systems can be utilized to minimize the curtailed wind energy [19]. A control method considering the minimization of the wind power curtailment and the reduction of transmission line flow congestion is proposed in [20]. Battery-based transportation systems and electric boilers can be used to reduce the wind curtailment in [21] and [22], respectively. Coordinated frequency control by synchronous generators, optimal wind curtailment, and VSC-HVDC systems is developed in [23]. An optimization formulation for the wind power suppression to enhance power system frequency stability is developed in [24]. The contributions of VSC-HVDC systems with virtual inertia control to reduce the amount of wind power curtailment considering frequency and DC voltage constraints are evaluated in [25] and [29], respectively.

The optimization of the wind power curtailment under low-voltage operation is discussed in [26], [27], and [28]. The priority of active/reactive current produced by a wind source during a voltage dip can be optimized [26]. The reactive power reserve of a wind farm is maximized for grid support during voltage events [27]. The shortfall of active power production by a wind farm triggered by a low-voltage event should be minimized [28]. However, the influence of this wind power curtailment on the main grid operation cost is not investigated in [26], [27], and [28].

Although these previous literatures have focused on the wind power curtailment techniques, the following aspects have not yet been covered:

1) The optimization of the wind power curtailment under low-voltage conditions considering the main grid operation cost has not been studied. When a grid-side fault occurs near the WPPs, the wind-side PCC bus voltage should be maintained. The controllability of converters in a wind turbine is aggravated during the voltage drop due to the converter current limiters. In addition, the WPPs can be disconnected from the grid-side if the voltage sag is not properly handled. This results in a critical frequency drop on the grid-side. Dynamic voltage control methods by wind generations can be implemented to mitigate this phenomenon. Nonetheless, the steady-state reactive power production from the wind generation is also helpful for voltage recovery if the dynamic voltage support is insufficient. However, the active power production of the wind generations should be reduced to guarantee the reactive power output.
   The system operation cost inevitably increases by the wind power curtailment. This curtailment should be carefully determined since it increases the generators' operation cost of the main grid. Nevertheless, the interaction between the main grid operation cost and the wind curtailment optimization is not studied in the previous works [26], [27], [28].
2) The reserve margin secured by the wind power curtailment can be utilized for various purposes. In addition to the pre-contingency reactive power production, the reserve can also be used for primary frequency control after the wind-side PCC bus voltage is sufficiently recovered. In other words, the wind power curtailment is useful for both voltage and frequency control in the case of voltage drop. None of the previous studies have evaluated the effectiveness of wind output suppression from these perspectives.

C. NOVEL CONTRIBUTION

The optimal wind power curtailment level considering the LVRT condition can be calculated by the OPF formulation. The OPF solution ensures stable power system operations by considering system constraints. These constraints include the safe operation limits of system models and the prevention of instability. In particular, the dynamic response of the power system can be analyzed in the stability analysis while optimizing the generator scheduling.

The PCC bus voltage of a wind generation model during low-voltage operation is handled as an additional constraint to guarantee a feasible operation. This approach can be adopted by system operators to determine an adequate amount of wind output suppression considering low-voltage operation.

The novel contribution points of this paper are summarized as follows:

1) A novel optimization formulation for the wind power curtailment under low-voltage conditions is developed. Compared to other works, the proposed method can determine the integrated operation scheduling of both generators and wind sources. The optimal suppression level of the wind power can be determined by considering the fuel cost minimization and wind-side PCC bus voltage constraint in the OPF analysis. Therefore, the impact of the wind power curtailment on the main grid operation cost can be investigated. In order to maintain the wind-side bus voltage within a feasible range under the LVRT condition, the wind-side voltage constraint is incorporated. Unlike our previous studies, the contribution of the reactive power output is considered to assess this aspect.
2) The primary frequency support of the wind model during low-voltage operation is proposed. In the case of a fault near the wind model, the wind power output is reduced due to the voltage drop. As a consequence,

the grid frequency near the wind generation decreases. The wind-side grid frequency controller can relieve this frequency drop if the PCC bus voltage is recovered sufficiently.

3) The effectiveness of the optimization methodology is validated with various wind-side voltage constraints and WPP capacity scenarios. The relationships between the wind curtailment level, voltage constraints, and WPP capacities are discussed.

The rest of this article is organized as follows. The wind power plant model is illustrated in Section II. The optimization formulation of the OPF is covered in Section III. The power system models are described in Section IV. The effectiveness of the proposed methodology is validated based on the simulation results in Section V.

II. WIND POWER PLANT MODEL WITH OUTPUT CURTAILMENT

A. WIND POWER PLANT MODEL

The model of the wind power plant is shown in FIGURE 2. The primary frequency control is implemented in the wind model [30]. VSC converters can be used on both rotor and grid sides. The active and reactive power output values of the wind model are assumed to follow the references immediately due to the rapid response speed of the converters [9].

The swing equation of the wind model is modeled as (1)-(2). The active power production of the wind model in (3) is calculated based on the coefficient C_{WT} and the rotational speed ω_r. C_{WT} can be obtained by the wind speed, wind blade radius, and rotor speed parameters.

The primary frequency controller (4) is adopted for the wind power plant model. If a frequency drop is observed, the active power production is adjusted by P_f based on the wind-side grid frequency measurement f_{WF}. The final active power output P_{WT} consists of P_{MPPT} and P_f in (5) – (6) [25].

$$2H_{WT}\omega_r \frac{d\omega_r}{dt} = P_{m,WT} - P_{WT}\ [p.u.] \tag{1}$$

$$\frac{d\omega_r}{dt} = \frac{1}{2H_{WT}\omega_r}(P_{m,WT} - P_{WT})\ [p.u.] \tag{2}$$

$$P_{MPPT} = C_{WT}\omega_r^3 \tag{3}$$

$$P_f = k_f(f_{WT,0} - f_{WT}) \tag{4}$$

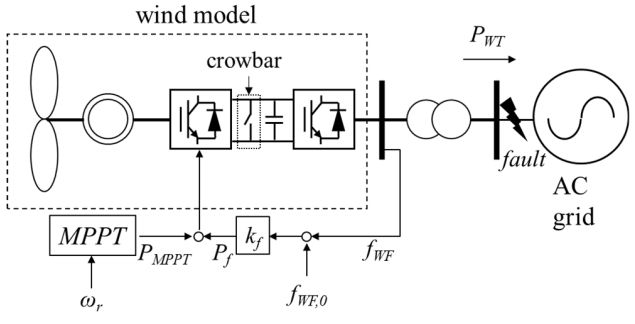

FIGURE 2. Model of wind power plant [9], [25].

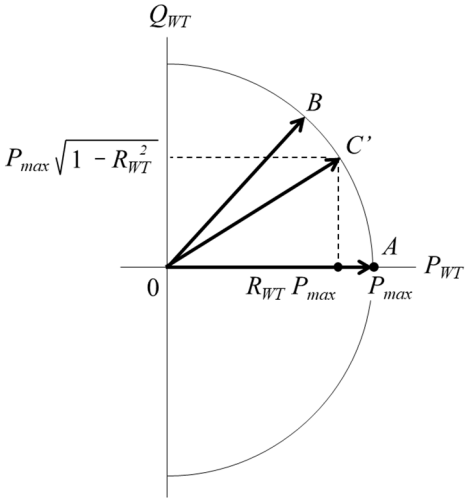

FIGURE 3. Wind power curtailment model.

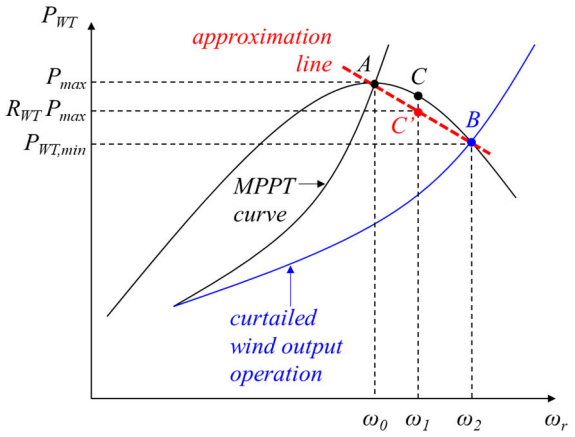

FIGURE 4. Rotor speed and wind power characteristics [9], [31].

$$P_{WT} = P_{MPPT} + P_f \tag{5}$$

$$P_{WT} = C_{WT}\omega_r^3 + k_f(f_{WF,0} - f_{WF}) \tag{6}$$

B. WIND POWER CURTAILMENT

The principle of the wind power curtailment is illustrated in FIGURE 3. The reserve capacity of the wind generation can be obtained by curtailing the wind power. If the active power output is suppressed by (1 - R_{WT})P_{max}, this capacity can be used as the reserve margin for the frequency control.

Furthermore, the wind power plant can produce a reactive power Q_{WT} using this capacity. If the active power output P_{WT} is equal to the maximum output P_{max}, the wind model cannot produce the reactive power output. On the contrary, the reactive power output can be produced by curtailing the active power output. This reactive power output can improve the grid-side voltage stability near the wind model.

The overspeed control method of ω_r can be adopted for the curtailed wind output operations [12]. In FIGURE 4, the

blue-solid curve corresponds to the deloaded wind output operation by the overspeed control. If the original operation point is A, the output of the wind power can be reduced from P_{max} to the minimum value of $P_{WT,min}$ at point B by increasing the rotor speed from ω_0 to ω_2. Hence, ω_2 corresponds to the maximum rotor speed for the deloaded operation. The curtailed operation point C exists between points A and B. The point C can be determined by the proposed formulation in Section III.

A linearly approximated equation can be used to represent the rotor speed and wind power characteristics around ω_1 [31]. The approximated behavior of the wind output curtailment is represented by the red-dotted line in FIGURE 4. In this case, the deloaded wind operation point C shifts to the new operation point C'.

C. LVRT METHOD OF WIND MODEL

The disconnection of a large-scale wind generation caused by a sudden voltage drop can have a negative impact on the power system frequency. LVRT is essential for the wind generator to prevent this phenomenon. The generators should be connected during the voltage drop.

On the other hand, this LVRT requirement is a critical burden from the viewpoint of the wind generation. A wind turbine is exposed to DC link overvoltage since the generated power cannot be delivered to the grid-side [32], [33]. Unlike the rotational speed of a wind turbine with slow inertial behavior, the DC link voltage rapidly increases. Therefore, effective solutions are required to deal with this DC link overvoltage.

One of the general LVRT methods for wind turbines is crowbar protection [32], [34]. A chopper circuit which is composed of resistors in FIGURE 5 is installed across the DC link capacitor, as noted in FIGURE 2. The chopper circuit does not operate under normal conditions. However, it is activated when the DC link overvoltage is measured. This chopper circuit helps dissipate the power imbalance during the voltage sag. The DC link voltage can be maintained within a safe range using this approach. In this regard, it is assumed that this chopper-based crowbar protection is applied to the LVRT of the wind model to maintain the DC link voltage within the stable operating range in this paper. Different state-of-the-art technologies can also be applied to avoid the DC link overvoltage. The results with various LVRT methods considering the detailed behavior of the DC link voltage can be explored in future topics.

In the case of voltage drop, a wind generation model is required to supply active power to the grid-side to avoid large frequency deviations. On top of that, the reactive power output of the wind source is necessary for effective voltage recovery. Therefore, the wind model should not be immediately disconnected when the voltage drop occurs. Power system operators have various grid codes for LVRT requirements depending on their grid characteristics.

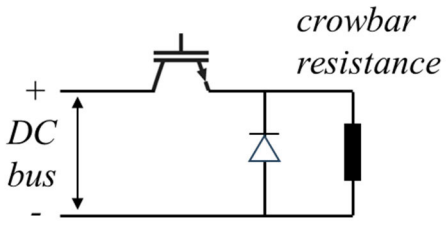

FIGURE 5. Crowbar protection circuit.

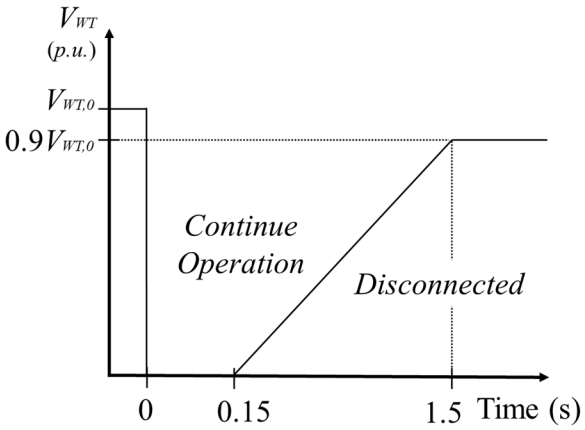

FIGURE 6. Low-voltage ride through requirement of wind model.

An example of the LVRT requirements adopted in this paper is shown in FIGURE 6. In case of a grid-side fault occurrence at $t = 0$ s, the wind-side PCC bus voltage V_{WT} drops from the pre-fault level $V_{WT,0}$ to zero. The voltage V_{WT} can be recovered if the fault is cleared properly. The LVRT requirement in FIGURE 6 indicates the wind model should be connected to the grid-side for 0.15 s even if V_{WT} is zero. The wind model disconnection is allowed if V_{WT} is lower than $0.9V_{WT,0}$ after 1.5 s.

On the other hand, this LVRT requirement results in the transient overcurrent of the wind model during a significant voltage drop. In order to avoid a severe overcurrent problem, the wind generation model can be protected by blocking its converter controller. In this article, the wind source is blocked when V_{WT} drops below the voltage criteria. The active and reactive power outputs of the wind model are zero while the converters are blocked.

III. OPTIMAL POWER FLOW WITH WIND-SIDE VOLTAGE CONSTRAINT

A. MATHEMATICAL FORMULATION

In general, the OPF model can be formulated in (7). The control variable vector u contains the active power outputs and the terminal bus voltage magnitudes of generators. The objective function (7a) is the total fuel cost of synchronous generators. The constraints for the pre-contingency state are modeled in (7b) and (7c). Similarly, the constraints (7d) and (7e) in the contingency case k within a pre-defined

contingency set K are considered.

$$f_0(x_o, u_o) = \sum_G (C_G + B_G P_G + A_G P_G^2) \tag{7a}$$
$$g_o(x_o, u_o) = 0 \tag{7b}$$
$$h_o(x_o, u_o) \leq 0 \tag{7c}$$
$$g_k(x_k, u_k) = 0;\ \forall k \in K \tag{7d}$$
$$h_k(x_k, u_k) \leq 0;\ \forall k \in K \tag{7e}$$

With regard to the equality constraint (7b), the active and reactive power balances at bus i are formulated in (8a) and (8b), respectively. In other words, the AC power flow model in the steady-state is considered in (7b).

The inequality constraints for the active, reactive, and apparent power outputs of the generators are shown in (8c) – (8e), respectively. The magnitude of AC bus voltage in the steady-state $V_{AC,0}$ is constrained between 0.9 *p.u.* and 1.1 *p.u.* in (8f). The transmission line power flow between buses i and j $P_{line,ij,0}$ and the ratio of tap transformer $R_{Tap,0}$ are limited by their respective operation limits in (8g) and (8h).

Regarding the wind model, the constraints for the active, reactive, and apparent power output values in the steady-state are included in (8i) – (8k). The maximum output limits of the active, reactive, and apparent power values are determined by the wind model capacity.

The wind power curtailment ratio can be treated as an additional control variable in the OPF formulation [25], [29]. The ratio of the wind power curtailment to the maximum wind power output is represented as R_{WT}. For instance, the active power production of a 500MW wind model is 450MW if $R_{WT,0}$ is 0.9. R_{WT}^{max} is one, which indicates that a wind power output suppression is not necessary. In this paper, R_{WT}^{min} is 0.9 so that up to 10% of wind power curtailment is allowed. This wind output curtailment constraint is incorporated into (8l).

$$P_{G,i,0} - P_{L,i,0} = \sum_{j \in E(i)} P_{ij,0};\ \forall i \in E(i) \tag{8a}$$
$$Q_{G,i,0} - Q_{L,i,0} = \sum_{j \in E(i)} Q_{ij,0};\ \forall i \in E(i) \tag{8b}$$
$$P_{G,i}^{\min} \leq P_{G,i,0} \leq P_{G,i}^{\max};\ \forall i \in E(i) \tag{8c}$$
$$Q_{G,i}^{\min} \leq Q_{G,i,0} \leq Q_{G,i}^{\max};\ \forall i \in E(i) \tag{8d}$$
$$S_{G,i}^{\min} \leq S_{G,i,0} \leq S_{G,i}^{\max};\ \forall i \in E(i) \tag{8e}$$
$$V_{AC,i}^{\min} \leq V_{AC,i,0} \leq V_{AC,i}^{\max};\ \forall i \in E(i) \tag{8f}$$
$$0 \leq P_{line,ij,0} \leq P_{line,ij}^{\max};\ \forall i,j \in E(i) \tag{8g}$$
$$R_{Tap}^{\min} \leq R_{Tap,0} \leq R_{Tap}^{\max} \tag{8h}$$
$$P_{WT}^{\min} \leq P_{WT,0} \leq P_{WT}^{\max} \tag{8i}$$
$$Q_{WT}^{\min} \leq Q_{WT,0} \leq Q_{WT}^{\max} \tag{8j}$$
$$S_{WT}^{\min} \leq S_{WT,0} \leq S_{WT}^{\max} \tag{8k}$$
$$R_{WT,0}^{\min} \leq R_{WT,0} \leq R_{WT,0}^{\max} \tag{8l}$$

The post-contingency equality and inequality constraints are explained as follows. The equality constraints (9a) and (9b) indicate the AC power flow model. The active, reactive, and apparent power production of the generators are limited in (9c) – (9e). The constraints for the transmission line flow and the tap transformer ratio are included in (9f) and (9g), respectively.

The active, reactive, and apparent power output values of the wind model are limited by their respective constraints in (9h) – (9j). On top of that, the wind-side PCC bus voltage constraint (9k) is considered. This represents that compared to the steady-state voltage $V_{WT,0}$, the wind-side PCC bus voltage deviation should not exceed $V_{WT,range}$ after the contingency clearance.

This OPF formulation with the voltage constraint (9k) considering the optimization of the wind power curtailment (8l) is a newly proposed approach, which is one of the novel contributions of this article. Basically, the dynamic voltage support of the wind model in FIGURE 1 is activated during a voltage dip. When the dynamic voltage control is not sufficient to satisfy the voltage constraint (9k), the wind power output can be curtailed by (8l) to secure the reactive power reserve capacity.

$$P_{G,i,k} - P_{L,i,k} = \sum_{j \in E(i)} P_{ij,k};\ \forall i \in E(i) \tag{9a}$$
$$Q_{G,i,k} - Q_{L,i,k} = \sum_{j \in E(i)} Q_{ij,k};\ \forall i \in E(i) \tag{9b}$$
$$P_{G,i}^{\min} \leq P_{G,i,k} \leq P_{G,i}^{\max};\ \forall i \in E(i) \tag{9c}$$
$$Q_{G,i}^{\min} \leq Q_{G,i,k} \leq Q_{G,i}^{\max};\ \forall i \in E(i) \tag{9d}$$
$$S_{G,i}^{\min} \leq S_{G,i,k} \leq S_{G,i}^{\max};\ \forall i \in E(i) \tag{9e}$$
$$0 \leq P_{line,ij,k} \leq P_{line,ij}^{\max};\ \forall i,j \in E(i) \tag{9f}$$
$$R_{Tap}^{\min} \leq R_{Tap,k} \leq R_{Tap}^{\max} \tag{9g}$$
$$P_{WT}^{\min} \leq P_{WT,k} \leq P_{WT}^{\max} \tag{9h}$$
$$Q_{WT}^{\min} \leq Q_{WT,k} \leq Q_{WT}^{\max} \tag{9i}$$
$$S_{WT}^{\min} \leq S_{WT,k} \leq S_{WT}^{\max} \tag{9j}$$
$$V_{WT,k} \leq V_{WT,0} \pm V_{WT,range} \tag{9k}$$

B. OPTIMIZATION METHOD

The pre-proposed optimization algorithm using the differential evolution method in [25] and [29] is adopted with several revisions. Compared to conventional mathematical approaches, this evolutionary method can incorporate the transient behaviors of power system models with high accuracy using time-domain simulation.

The description for the optimization algorithm is provided in FIGURE 7. The set of control vectors u is randomly initialized. The steady-state feasibility of each control vector can be verified by the power flow analysis.

In the case of the steady-state constraints violence in (8), the vector is considered as an infeasible vector. In other words, the infeasible generator operations and the wind curtailment level cannot be accepted by system operators.

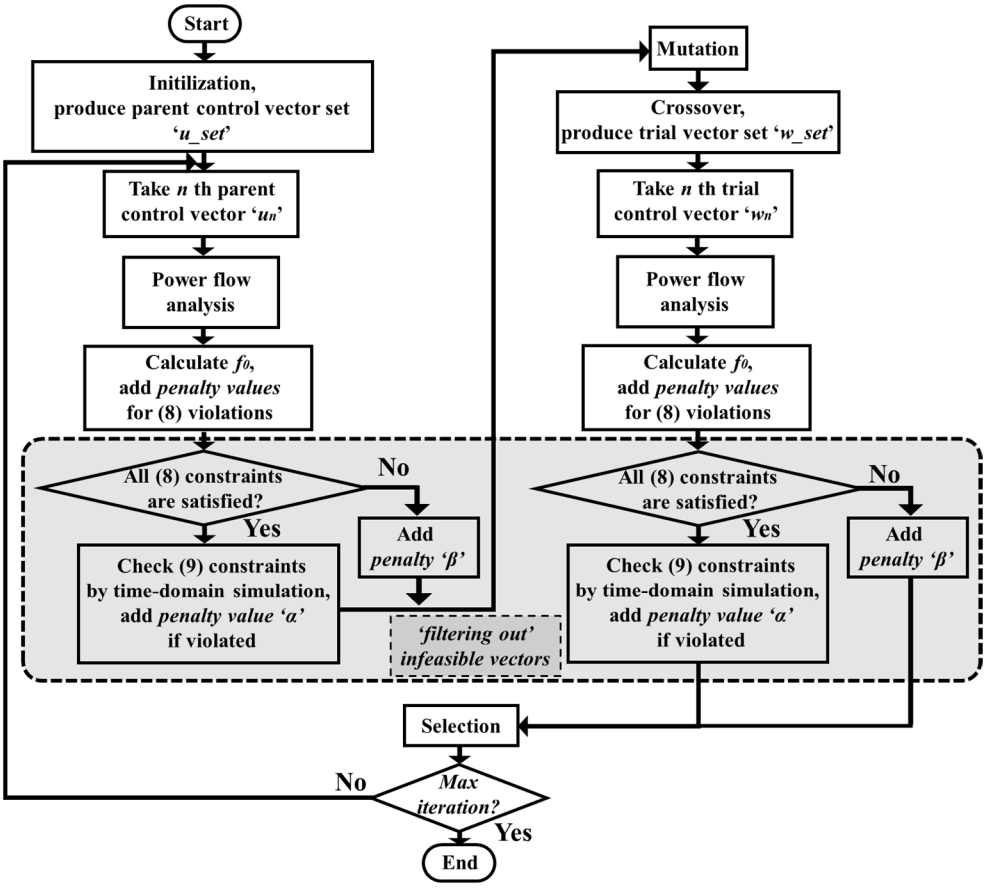

FIGURE 7. Algorithm of OPF analysis [25], [29].

Consequently, the fitness value is increased by a large penalty β to avoid the infeasible operation.

The post-contingency feasibility of the control vector is verified by the time-domain simulation. The control vector is checked to determine whether it satisfies all post-contingency constraints in (9). A penalty α is imposed on the fitness value if one of the constraints in (9) is violated.

In the mutation stage, the set of trial vectors w is produced. The entire procedure is also performed for all trial vectors. Between the control and trial vectors, the one which has the lower fitness value is selected as the new control vector. This evolutionary process is repeated until the number of iterations exceeds the maximum iteration limit.

As for the scales of penalty values α and β, it has been discussed in [25] and [29] that β should be much larger than α for the effective filtering-out process. A control vector penalized by β should not be chosen in the selection stage. The time-domain simulation is not carried out if the vector is penalized by β to reduce the computational burden. For example, the penalty value β is 100 times larger than α, and the scale of α can be 100 times larger than the expected objective function value [25], [29].

IV. POWER SYSTEM MODELS

The Western System Coordinating Council (WSCC) three-generator nine-bus system and IEEE-39 bus system models with the wind model installations are adopted for the simulation analysis, as described in FIGURE 8 and FIGURE 9, respectively. As regards the wind model, the fuel cost coefficients are considered to be zero. The wind power curtailment of up to 10% of the rated power output is allowed [25], [35]. In other words, the minimum R_{WT} value is 0.9. For instance, the active power production of a 1000MW wind power plant can be suppressed by 100MW. As a consequence, the maximum output of reactive power Q_{WT} of the 1000MW wind power plant model is 435.9MVAR.

A symmetrical three-phase fault near the wind model is considered as the disturbance type, which is cleared after 70ms. The fuel cost coefficient values of the synchronous generators in [36] can be used for the objective function calculation. The lower and upper constraints for the active power outputs of the synchronous generators are provided in the Appendix. The generators have the automatic voltage regulator (AVR) and turbine speed governor (GOV) models, as described in [37] and [38]. The detailed description of the models is provided in the Appendix.

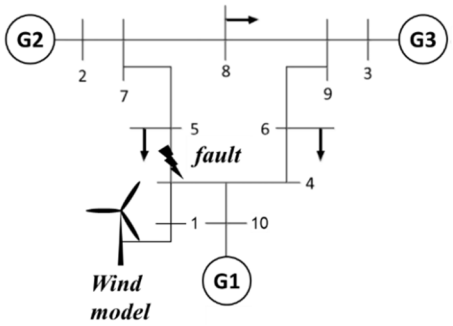

FIGURE 8. System model 1 - three-generator nine-bus system with wind model.

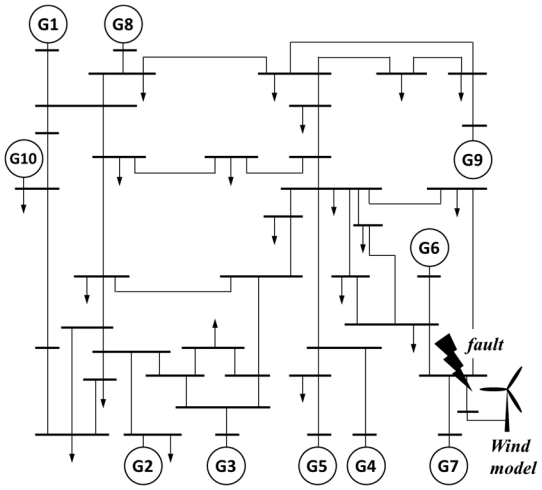

FIGURE 9. System model 2 - IEEE 39-bus system with wind model.

As for the fault location, the fault occurrence at the wind-side PCC bus is considered in both system models to simulate the most significant voltage drop scenarios from the wind generation perspective. This aims to guarantee feasible system operations against any wind-side bus voltage fluctuations.

V. SIMULATION RESULTS AND DISCUSSION

A. EVALUATION ON THE PROPOSED METHODOLOGY

The performance of the proposed scheme is evaluated using the test system models. A three-phase symmetrical fault occurs at $t = 1$ s. In the case of a severe grid-side fault occurrence, the wind generation should be protected by blocking converter control. Hence, the active and reactive power outputs of the wind model are zero when the wind-side PCC bus voltage V_{WT} is less than 0.2 *p.u.* in this paper. The simulations are performed using the MATLAB/Simulink software.

The post-contingency trajectories in the WSCC nine-bus system are plotted from FIGURE 10 to FIGURE 13. The wind-side PCC bus voltage V_{WT} decreases to zero at 1 s as plotted in FIGURE 10. Two case scenarios are simulated depending on the activation of the wind-side grid frequency controller. The frequency controller can be activated if V_{WT} is sufficiently recovered above 0.9 *p.u.*. It can be seen that the

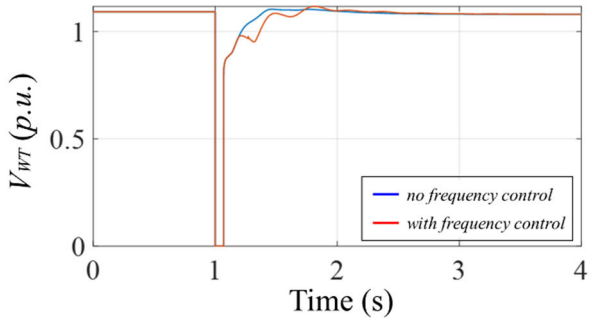

FIGURE 10. Wind-side PCC bus voltage V_{WT} (system model 1).

recovery speed of V_{WT} above 0.9 *p.u* becomes slower if the frequency control is utilized. Instead, the frequency drop of G1 near the wind model can be reduced. This can be achieved from the reserve margin of the wind model obtained by the wind power curtailment. When the active power output of the wind model P_{WT} is deloaded, it can provide the reserve margin for the frequency control.

The behavior of the reactive power output Q_{WT} can be explained as follows. The reactive power output is zero since the converters of the wind model are blocked during the fault occurrence. The reactive power output control is allowed after the fault clearance in FIGURE 13. The output is reduced as the voltage V_{WT} recovers to the pre-fault state.

Meanwhile, the reactive power production of the wind power plant model Q_{WT} decreases compared to the pre-fault value during the wind-side grid frequency control, as described in FIGURE 13. This results in the voltage recovery difference of V_{WT} in FIGURE 10.

The results of the IEEE 39-bus system model shown from FIGURE 14 to FIGURE 17 can be explained similarly. The wind-side grid frequency control leads to the difference in V_{WT} recovery characteristics, as illustrated in FIGURE 14. In order to apply the frequency control, the reactive power output Q_{WT} in FIGURE 17 should be temporarily reduced. Consequently, the frequency nadir of G7 near the wind model can increase compared to the case without the frequency control.

In FIGURE 13 and FIGURE 17, there are no reactive power oscillations in the '*no frequency control*' cases. On the other hand, the oscillations are observed when the frequency control of the wind model is activated. The power system frequency can fluctuate after the fault occurrence. If frequency control is adopted, the active power output of the wind model P_{WT} is controlled based on the system frequency fluctuation. Due to the maximum apparent power output constraint of the wind model in (9j), the reactive power output Q_{WT} is limited and varies depending on the active power output P_{WT} and the wind model capacity.

B. SENSITIVITY ANALYSIS ON WIND-SIDE VOLTAGE CONSTRAINTS

The relationship between the wind power curtailment ratio, the main grid fuel costs, and the wind-side PCC bus voltage

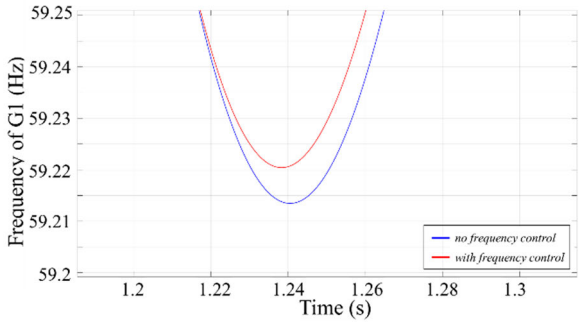

FIGURE 11. Frequency nadir of G1 (system model 1).

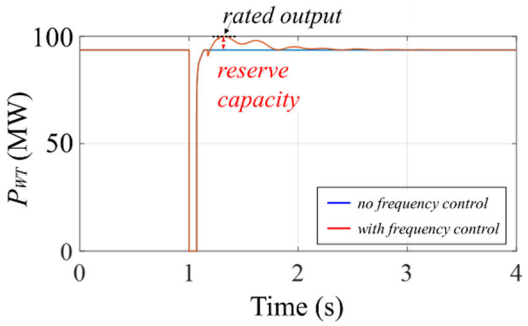

FIGURE 12. Active power output P_{WT} of wind model (system model 1).

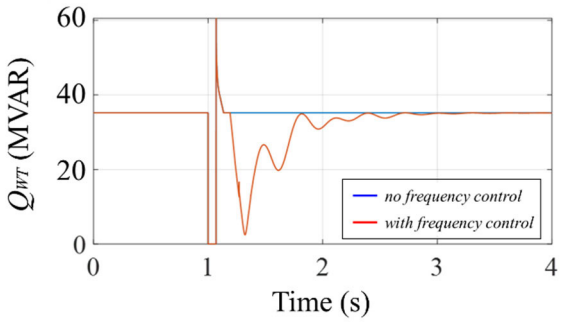

FIGURE 13. Reactive power output Q_{WT} of wind model (system model 1).

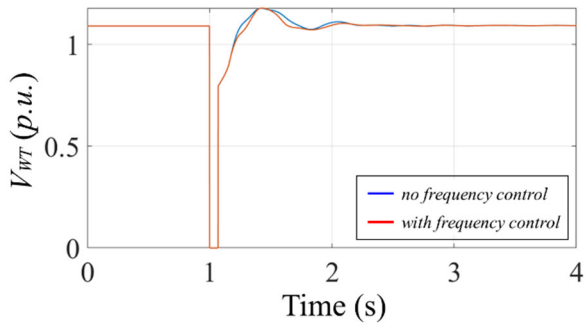

FIGURE 14. Wind-side PCC bus voltage V_{WT} (system model 2).

constraint is discussed. The curtailment ratio values of the wind power R_{WT} are listed in Table 1. The symbol 'X' represents a feasible solution cannot be obtained.

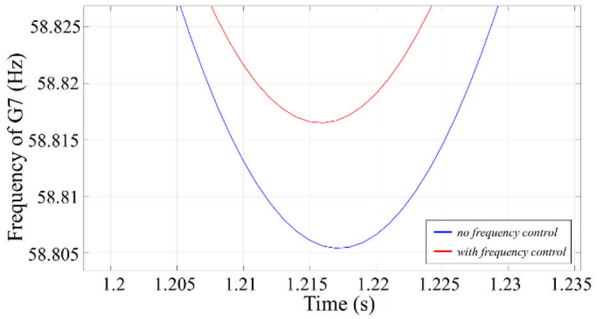

FIGURE 15. Frequency nadir of G7 (system model 2).

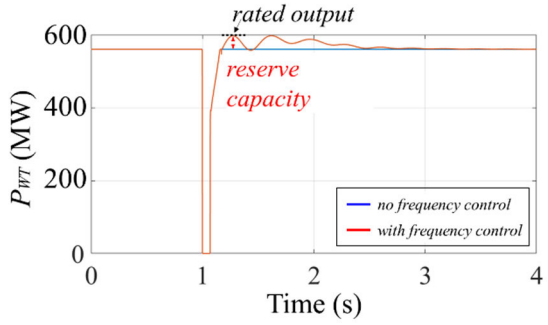

FIGURE 16. Active power output P_{WT} of wind model (system model 2).

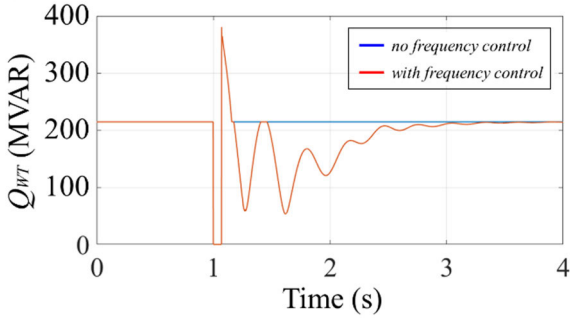

FIGURE 17. Reactive power output Q_{WT} of wind model (system model 2).

As regards the WSCC nine-bus power system model, R_{WT} is 0.998 when the wind-side voltage constraint $V_{WT,range}$ is 0.20 *p.u.*. The value of R_{WT} decreases as $V_{WT,range}$ decreases. The fuel cost f_0 increases as R_{WT} reduces. In order to satisfy the wind-side PCC bus voltage constraint, the wind power plant should produce more reactive power as $V_{WT,range}$ is reduced. Hence, the lowest optimal value R_{WT} 0.936, is calculated when $V_{WT,range}$ is 0.16 *p.u.*. When $V_{WT,range}$ is less than 0.15 *p.u.*, the feasible solution is not obtained due to the strict wind-side voltage constraint.

A similar tendency can be observed in the IEEE 39-bus system model results, as listed in Table 2. Compared to the result of $V_{WT,range} = 0.25$ *p.u.*, the optimal value of R_{WT} decreases as the wind-side PCC bus voltage constraint $V_{WT,range}$ becomes stricter. The lowest fuel cost 54000 \$/hour can be obtained in the highest R_{WT} of 0.991. The

TABLE 1. Ratio of curtailed wind power output R_{WT} with different voltage constraints (System model 1).

$V_{WT,range}$	R_{WT}	*Fuel cost* f_0 (\$ / hour)
0.20	0.998	607
0.19	0.996	609
0.18	0.989	612
0.17	0.972	617
0.16	0.936	625
0.15	X	

TABLE 2. Ratio of curtailed wind power output R_{WT} with different voltage constraints (System model 2).

$V_{WT,range}$	R_{WT}	*Fuel cost* f_0 (\$ / hour)
0.25	0.991	54000
0.24	0.987	54070
0.23	0.986	54185
0.22	0.983	54315
0.21	0.966	54590
0.20	0.934	54850
0.19	X	

optimal curtailed wind output ratio R_{WT} for $V_{WT,range} = 0.20$ *p.u.* is 0.934. The solution is not found when $V_{WT,range}$ is 0.19 *p.u.*.

C. SENSITIVITY ANALYSIS ON CAPACITY OF WIND MODEL

Case studies with various capacities of the wind model are analyzed. The R_{WT} results for the ratio of the deloaded wind power output and the fuel costs are presented in Table 3 and Table 4. Regarding the wind-side voltage constraint, $V_{WT,range}$ criteria are fixed to be 0.17 *p.u.* in the WSCC nine-bus power system model and 0.20 *p.u.* in the IEEE 39-bus system model, respectively.

The wind active power can be calculated by multiplying the wind capacity and R_{WT}. First of all, the wind active power output consistently increases in all wind capacity ranges in both system models. Therefore, the fuel cost results reduce as the wind capacity increases.

In Table 3, the optimal ratio of R_{WT} is 0.916 with an 80MW wind power plant model. As the capacity of the wind model increases to 200MW, the optimal value of R_{WT} also increases. Provided that the wind-side voltage constraint $V_{WT,range}$ can be satisfied by the reactive power production Q_{WT}, the wind power plant model is required to maximize the active power production P_{WT} to minimize the fuel cost in the OPF analysis.

It is noteworthy that R_{WT} decreases from one to 0.968 when the wind model capacity is 240MW. A feasible solution is not obtained in the case of a 250MW wind model. The voltage stability of the grid-side can be aggravated as the active power flow on the load bus increases. In such a case, reactive power compensation by the wind power plant model can relieve

TABLE 3. Ratio of curtailed wind power output R_{WT} with different wind model capacities (System model 1, $V_{WT,range} = 0.17$).

Wind capacity (MW)	R_{WT}	Wind active power (MW)	*Fuel cost* f_0 (\$ / hour)
80	0.916	73.3	669
90	0.952	85.7	641
100	0.972	97.2	617
120	0.989	119	571
200	1	200	405
240	0.968	232	344
250		X	

TABLE 4. Ratio of curtailed wind power output R_{WT} with different wind model capacities (System model 2, $V_{WT,range} = 0.20$).

Wind capacity (MW)	R_{WT}	Wind active power (MW)	*Fuel cost* f_0 (\$ / hour)
600	0.934	560.4	54850
700	0.950	665.0	53160
800	0.966	772.8	51570
900	0.971	873.9	50020
1000	0.953	953.0	48867
1050	0.908	953.4	48857
1100		X	

this phenomenon. Thus, the pre-contingency reactive power production of the wind power plant model increases and the active power output should be curtailed.

A similar tendency is observed in Table 4. The optimal deloaded wind power output ratio R_{WT} is 0.932 when the capacity of the wind power plant model is 600MW. The level of wind output curtailment can be reduced as the capacity increases to 900MW. On the contrary, the grid-side voltage stability near the wind model is aggravated when the wind capacity is above 1000MW. The wind power plant is required to provide the reactive power compensation to satisfy the wind-side voltage constraint. The active power production P_{WT} of the wind power plant should be suppressed. A feasible solution is not found when the wind capacity is 1100MW since the wind-side voltage constraint cannot be satisfied.

VI. CONCLUSION

The formulation of the optimized wind power output curtailment for the LVRT condition is proposed. The optimized wind power curtailment level can be determined considering the minimization of the fuel cost and the wind-side PCC bus voltage constraints. As the wind power output is suppressed, the fuel costs of power system models increase. Based on the wind-side reserve capacity, the reactive power output of the wind model can be controlled, which helps satisfy the wind-side PCC bus voltage constraints. The reactive power

output is determined based on the rated wind power output and the optimized wind power curtailment ratio. In addition, the wind model is equipped with the frequency controller to deal with the frequency drop during low-voltage operation. The relationships among the wind power curtailment ratio, the wind-side voltage constraint, and the wind model capacity are analyzed. It is revealed that the wind power curtailment increases when the voltage constraint becomes stricter. As the capacity of the wind model increases, the curtailment level decreases. However, the curtailment level increases when the wind capacity exceeds the threshold capacity.

In the future, the detailed characteristics of the wind model DC link voltage using the proposed methodology will be analyzed. Different wind-side frequency and dynamic voltage controllers can be implemented to investigate the impacts on the wind curtailment results since the results can differ depending on the performance of the controllers. The proposed methodology can be applied to grids with multiple wind models. Furthermore, the contribution of HVDC transmission systems can be discussed.

APPENDIX

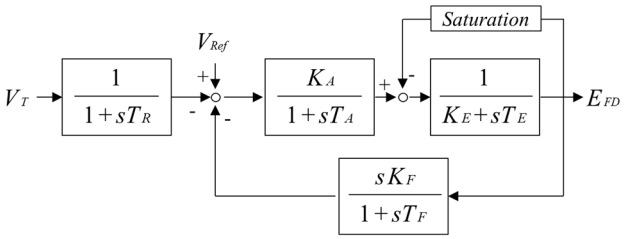

FIGURE 18. AVR model - IEEE Type 1 excitation model [37].

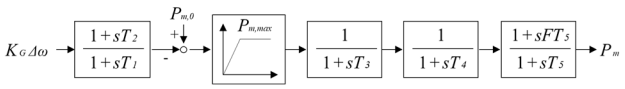

FIGURE 19. Turbine-governor model [38].

TABLE 5. AVR model parameters of nine-bus system (System model 1).

	T_R (s)	K_A	T_A (s)	K_E	T_E (s)	K_F	T_F (s)
G1	1	100	0.395	1	0	0.0635	1
G2	1	100	0.395	1	0	0.0635	1
G3	1	100	0.395	1	0	0.0635	1

TABLE 6. Turbine-governor model parameters of nine-bus system (System model 1).

	K_G	T_1 (s)	T_2 (s)	T_3 (s)	T_4 (s)	T_5 (s)	F
G1	2	0.2	0.4	0.3	0	10	0.3
G2	2	0.2	0.4	0.3	0	10	0.3
G3	2	0.2	0.4	0.3	0	10	0.3

TABLE 7. AVR model parameters of IEEE 39-bus system (System model 2).

	T_R (s)	K_A	T_A (s)	K_E	T_E (s)	K_F	T_F (s)
G1	1	200	0.358	1	0.004	0.0529	1
G2	1	400	0.0200	1	0.942	0.0300	1
G3	1	400	0.0200	1	0.942	0.0300	1
G4	1	400	0.0200	1	0.942	0.0300	1
G5	1	400	0.0200	1	0.942	0.0300	1
G6	1	400	0.0200	1	0.942	0.0300	1
G7	1	400	0.0200	1	0.942	0.0300	1
G8	1	400	0.0200	1	0.942	0.0300	1
G9	1	50	0.0600	-0.0393	0.440	0.0700	1
G10	1	50	0.0600	1	0.942	0.0300	1

TABLE 8. Turbine-governor model parameters of IEEE 39-bus system (System model 2).

	K_G	T_1 (s)	T_2 (s)	T_3 (s)	T_4 (s)	T_5 (s)	F
G1	5	0.2	0.4	0.3	0	10	0.3
G2	5	0.2	0.4	0.3	0	10	0.3
G3	5	0.2	0.4	0.3	0	10	0.3
G4	5	0.2	0.4	0.3	0	10	0.3
G5	5	0.2	0.4	0.3	0	10	0.3
G6	5	0.2	0.4	0.3	0	10	0.3
G7	5	0.2	0.4	0.3	0	10	0.3
G8	5	0.2	0.4	0.3	0	10	0.3
G9	5	0.2	0.4	0.3	0	10	0.3
G10	5	0.2	0.4	0.3	0	10	0.3

TABLE 9. Active power output constraints of nine-bus system (System model 1).

	$P_{G,min}$ (MW)	$P_{G,max}$ (MW)
G1	51.2	512
G2	27.0	270
G3	12.5	125

TABLE 10. Active power output constraints of IEEE 39-bus system (System model 2).

	$P_{G,min}$ (MW)	$P_{G,max}$ (MW)
G1	295	590
G2	418	835
G3	418	835
G4	418	835
G5	418	835
G6	418	835
G7	418	835
G8	418	835
G9	456	911
G10	456	911

REFERENCES

[1] H. Polinder, F. F. A. Van Der Pijl, G.-J. De Vilder, and P. J. Tavner, "Comparison of direct-drive and geared generator concepts for wind turbines," *IEEE Trans. Energy Convers.*, vol. 21, no. 3, pp. 725–733, Sep. 2006.

[2] M. Chinchilla, S. Arnaltes, and J. C. Burgos, "Control of permanent-magnet generators applied to variable-speed wind-energy systems connected to the grid," *IEEE Trans. Energy Convers.*, vol. 21, no. 1, pp. 130–135, Mar. 2006.

[3] H. Geng, L. Liu, and R. Li, "Synchronization and reactive current support of PMSG-based wind farm during severe grid fault," *IEEE Trans. Sustain. Energy*, vol. 9, no. 4, pp. 1596–1604, Oct. 2018.

[4] M. Nasiri and R. Mohammadi, "Peak current limitation for grid side inverter by limited active power in PMSG-based wind turbines during different grid faults," *IEEE Trans. Sustain. Energy*, vol. 8, no. 1, pp. 3–12, Jan. 2017.

[5] L. S. Vargas, G. Bustos-Turu, and F. Larraín, "Wind power curtailment and energy storage in transmission congestion management considering power plants ramp rates," *IEEE Trans. Power Syst.*, vol. 30, no. 5, pp. 2498–2506, Sep. 2015.

[6] D. Ochoa and S. Martinez, "Fast-frequency response provided by DFIG-wind turbines and its impact on the grid," *IEEE Trans. Power Syst.*, vol. 32, no. 5, pp. 4002–4011, Sep. 2017.

[7] X. Zhang, X. Zha, S. Yue, and Y. Chen, "A frequency regulation strategy for wind power based on limited over-speed de-loading curve partitioning," *IEEE Access*, vol. 6, pp. 22938–22951, 2018.

[8] J. W. Choi, S. Y. Heo, and M. K. Kim, "Hybrid operation strategy of wind energy storage system for power grid frequency regulation," *IET Gener., Transmiss. Distrib.*, vol. 10, no. 3, pp. 736–749, Feb. 2016.

[9] X. Zhang, Y. Chen, Y. Wang, X. Zha, S. Yue, X. Cheng, and L. Gao, "Deloading power coordinated distribution method for frequency regulation by wind farms considering wind speed differences," *IEEE Access*, vol. 7, pp. 122573–122582, 2019.

[10] G. Tu, Y. Li, and J. Xiang, "Coordinated rotor speed and pitch angle control of wind turbines for accurate and efficient frequency response," *IEEE Trans. Power Syst.*, vol. 37, no. 5, pp. 3566–3576, Sep. 2022.

[11] W. Bao, L. Ding, Y. C. Kang, and L. Sun, "Closed-loop synthetic inertia control for wind turbine generators in association with slightly over-speeded deloading operation," *IEEE Trans. Power Syst.*, vol. 38, no. 6, pp. 5022–5032, Nov. 2022.

[12] H. Luo, Z. Hu, H. Zhang, and H. Chen, "Coordinated active power control strategy for deloaded wind turbines to improve regulation performance in AGC," *IEEE Trans. Power Syst.*, vol. 34, no. 1, pp. 98–108, Jan. 2019.

[13] S. Konstantinopoulos and J. H. Chow, "Active power control of DFIG wind turbines for transient stability enhancement," *IEEE Open Access J. Power Energy*, vol. 10, pp. 208–221, 2023.

[14] C. Zhong, J. Zhang, and Y. Zhou, "Adaptive virtual capacitor control for MTDC system with deloaded wind power plants," *IEEE Access*, vol. 8, pp. 190582–190595, 2020.

[15] Z. Dong, Z. Li, Y. Dong, S. Jiang, and Z. Ding, "Fully-distributed deloading operation of DFIG-based wind farm for load sharing," *IEEE Trans. Sustain. Energy*, vol. 12, no. 1, pp. 430–440, Jan. 2021.

[16] S. Baros and M. D. Ilic, "Distributed torque control of deloaded wind DFIGs for wind farm power output regulation," *IEEE Trans. Power Syst.*, vol. 32, no. 6, pp. 4590–4599, Nov. 2017.

[17] C. Kim and W. Kim, "Low-voltage ride-through coordinated control for PMSG wind turbines using de-loaded operation," *IEEE Access*, vol. 9, pp. 66599–66606, 2021.

[18] B. Yang, X. Cao, Z. Cai, T. Yang, D. Chen, X. Gao, and J. Zhang, "Unit commitment comprehensive optimal model considering the cost of wind power curtailment and deep peak regulation of thermal unit," *IEEE Access*, vol. 8, pp. 71318–71325, 2020.

[19] H. Bitaraf and S. Rahman, "Reducing curtailed wind energy through energy storage and demand response," *IEEE Trans. Sustain. Energy*, vol. 9, no. 1, pp. 228–236, Jan. 2018.

[20] V. V. G. Krishnan, S. Gopal, R. Liu, A. Askerman, A. Srivastava, D. Bakken, and P. Panciatici, "Resilient cyber infrastructure for the minimum wind curtailment remedial control scheme," *IEEE Trans. Ind. Appl.*, vol. 55, no. 1, pp. 943–953, Jan. 2019.

[21] Z. Zhang, D. Mei, H. Jiang, G. Liu, H. He, and Y. Chen, "Mode for reducing wind curtailment based on battery transportation," *J. Modern Power Syst. Clean Energy*, vol. 6, no. 6, pp. 1158–1171, Nov. 2018.

[22] Y. Ma, Y. Yu, and Z. Mi, "Accommodation of curtailed wind power by electric boilers equipped in different locations of heat-supply network for power system with CHPs," *J. Modern Power Syst. Clean Energy*, vol. 9, no. 4, pp. 930–939, Jul. 2021.

[23] J.-S. Kim, Y.-J. Kim, and O. Gomis-Bellmunt, "Optimal frequency regulation of multi-terminal HVDC-linked grids with deloaded offshore wind farms control," *IEEE Trans. Sustain. Energy*, vol. 15, no. 1, pp. 290–303, Jan. 2024.

[24] S. Lim and J.-W. Park, "Enhancing frequency stability for grid resilience based on effective WPPs power curtailment," *IEEE Trans. Ind. Appl.*, vol. 60, no. 2, pp. 2302–2311, Mar. 2024.

[25] S. Kim, "Analysis of deloaded wind power in hybrid AC/HVDC systems by frequency stability constrained optimal power flow," *IEEE Access*, vol. 11, pp. 104441–104451, 2023.

[26] H. Karbouj and Z. H. Rather, "A novel wind farm control strategy to mitigate voltage dip induced frequency excursion," *IEEE Trans. Sustain. Energy*, vol. 10, no. 2, pp. 637–645, Apr. 2019.

[27] A. K. Bhyri, N. Senroy, and T. K. Saha, "Enhancing the grid support from DFIG-based wind farms during voltage events," *IEEE Trans. Power Syst.*, vol. 39, no. 1, pp. 733–744, Jan. 2024.

[28] X. Lyu, Y. Jia, T. Liu, and Y. He, "Concurrent optimal re/active power control for wind farms under low-voltage-ride-through operation," *IEEE Trans. Power Syst.*, vol. 35, no. 6, pp. 4956–4959, Nov. 2020.

[29] S. Kim, "Optimization of wind power curtailment by OPF in hybrid AC/VSC-HVDC systems with DC voltage constraints," *IEEE Access*, vol. 11, pp. 130828–130839, 2023.

[30] M. Mehrabankhomartash, M. Saeedifard, and A. Yazdani, "Adjustable wind farm frequency support through multi-terminal HVDC grids," *IEEE Trans. Sustain. Energy*, vol. 12, no. 2, pp. 1461–1472, Apr. 2021.

[31] R. G. de Almeida, E. D. Castronuovo, and J. A. PecasLopes, "Optimum generation control in wind parks when carrying out system operator requests," *IEEE Trans. Power Syst.*, vol. 21, no. 2, pp. 718–725, May 2006.

[32] O. P. Mahela, N. Gupta, M. Khosravy, and N. Patel, "Comprehensive overview of low voltage ride through methods of grid integrated wind generator," *IEEE Access*, vol. 7, pp. 99299–99326, 2019.

[33] R. Basak, G. Bhuvaneswari, and R. R. Pillai, "Low-voltage ride-through of a synchronous generator-based variable speed grid-interfaced wind energy conversion system," *IEEE Trans. Ind. Appl.*, vol. 56, no. 1, pp. 752–762, Jan. 2020.

[34] L. Yang, Z. Xu, J. Ostergaard, Z. Y. Dong, and K. P. Wong, "Advanced control strategy of DFIG wind turbines for power system fault ride through," *IEEE Trans. Power Syst.*, vol. 27, no. 2, pp. 713–722, May 2012.

[35] P. Mahish and A. K. Pradhan, "Distributed synchronized control in grid integrated wind farms to improve primary frequency regulation," *IEEE Trans. Power Syst.*, vol. 35, no. 1, pp. 362–373, Jan. 2020.

[36] T. B. Nguyen and M. A. Pai, "Dynamic security-constrained rescheduling of power systems using trajectory sensitivities," *IEEE Trans. Power Syst.*, vol. 18, no. 2, pp. 848–854, May 2003.

[37] P. Demetriou, M. Asprou, J. Quiros-Tortos, and E. Kyriakides, "Dynamic IEEE test systems for transient analysis," *IEEE Syst. J.*, vol. 11, no. 4, pp. 2108–2117, Dec. 2017.

[38] X. Zhao, H. Wei, J. Qi, P. Li, and X. Bai, "Frequency stability constrained optimal power flow incorporating differential algebraic equations of governor dynamics," *IEEE Trans. Power Syst.*, vol. 36, no. 3, pp. 1666–1676, May 2021.

SANGWON KIM (Member, IEEE) received the B.E. degree in electronic and electrical engineering from Sungkyunkwan University, Suwon, Republic of Korea, in 2015, and the M.E. and Dr.Eng. degrees in electrical engineering and information systems from The University of Tokyo, Japan, in 2017 and 2020, respectively. He was a Staff Engineer at the Department of Global Manufacturing and Infrastructure, Samsung Electronics, Republic of Korea, from 2020 to 2022. He is currently working as an Assistant Professor with the University of Ulsan, Ulsan, Republic of Korea. His research interests include power system operation and stability analysis including HVDC systems and renewable energy integration.